Hildebrand Award Symposium Lecture
[ACS meeting, San Francisco, April 3, 2017]

Hard Spheres under Gravity

Abstract: A very wide range of gravitational field strengths is present throughout our universe. Basic questions and problems arise about the effects of these fields and of their centrifugal analogs on the spatial distribution of matter. To illustrate a few of these issues, this lecture will describe the gravitational field behavior of the venerable classical hard sphere model (and of its 2-dimensional hard disk version). Properties to be discussed include (a) the barometric formula and its corrections, (b) crystal phase orientation, (c) isotope separation, and (d) jammed particle configurations formed by a dissipative sedimentation process.

Hard spheres have played a prominent role in the original research created by this year's Hildebrand Award recipient, Sal Torquato. Therefore it is appropriate to include some novel aspects of that model in this lecture. In particular, attention will be focused on gravitational effects and their centrifugal equivalents for the classical hard sphere model, as well as for its two-dimensional hard disk analog. These phenomena have received relatively limited attention in statistical mechanics, so this presentation will attempt to emphasize some of the more notable qualitative aspects, and will identify at least a few basic opportunities for future research.

View 1. Title. Lecturer name and affiliation. Acknowledgements.

The next View 2 identifies some very diverse examples of gravitational

---

View 2. Gravitational and centrifugal force field examples.

(and centrifugal) force field strengths across our universe. In the present context it is useful to illustrate at least one characteristic of these examples related to the spatial distribution of matter. Specifically, the following View 3 provides the elevation increases involved for a single ^{132}Xe atom residing

---

View 3. ^{132}Xe elevation changes requiring gravitational energy $k_BT\,|_{298K}$.

---

respectively in each of those View 2 field examples (assumed to be spatially homogeneous) that require an energy input equal to $k_B T$ at room temperature 298K. This is the most abundant of the nine stable isotopes of Xe. That particular element was chosen for illustration on account of its hard-sphere-like spherical symmetry, its near-classical behavior in many circumstances, and its stable crystal form equivalent to that of the hard sphere model. Of course unlike the hard sphere model, Xe isotopes and their mixtures exhibit a liquid-vapor transition at sufficiently low temperature and high particle density.

The obvious starting points for examination of gravitational/centrifugal field effects are the equilibrium macroscopic equations of state for the sphere and disk systems in the absence of those external fields. Because these are classical many-hard-particle systems their density-dependent pressures are strictly proportional to absolute temperature T. The hard sphere case shown in View 4 exhibits a conventional first-order melting-

---

View 4. Classical hard sphere equilibrium equation of state ($g = 0$). Nearest-neighbor separation at melting, and at close packing.

---

freezing transition, where the stable crystal structure has been determined to be face-centered cubic, but only by a small free energy favorability compared to the hexagonal close-packed alternative. View 5 presents the

---

View 5. Classical hard disk equilibrium equation of state ($g = 0$). Nearest-neighbor separation at melting, and at close packing. Hexatic phase.

---

analogous gravity-free hard disk equation of state which involves a considerably smaller melting-transition density jump. But it also exhibits an additional complicating feature, a very narrow hexatic phase density interval inserted between the fluid and the "conventional" crystal phase. In slight contrast with the well-known KTHNY theory of hexatic phases, the fluid-hexatic transition is first order, while the hexatic-crystal transition is higher order (as in the KTHNY description).

The following View 6 shows the macroscopic system container geometry

---

View 6. Macroscopic container geometry, field-oriented. Impenetrable floor (z_f) and ceiling (z_c) surfaces. Constant horizontal cross section area (or length) A. $\Phi_g(\mathbf{r}_1 ... \mathbf{r}_N)$. Boundary conditions are periodic for lateral

directions. Vertical pressure expression in terms of weight above measurement position, and the ceiling pressure.

---

to be used for the following analysis of the three-dimensional case, specifically a vertically oriented rectangular solid with constant horizontal cross-section area *A*. The number of contained spherical particles *N* will be fixed, with a canonical ensemble for description of thermal equilibrium states. The gravitational potential energy function $\Phi_g(\mathbf{r}_1 ... \mathbf{r}_N)$ for the *N* mass-*m* particles, measured from the floor position, has been included. The floor and ceiling flat surfaces, perpendicular to the gravitational force direction, will be impenetrable. The side walls could also be chosen as impenetrable, but here and for the remainder of the lecture we invoke the option of lateral direction periodic boundary conditions to eliminate wall interface effects. The two dimensional version, with a vertically oriented rectangular container enclosing *N* disks, is obvious. A general expression has also been included in the View for the altitude variation of the vertical pressure in terms of the ceiling pressure plus the *z*-dependent weight of the particle mass distribution above the observation position.

When the external gravitational or centrifugal field is weak, the thermal equilibrium spatial distribution of the particles within the fluid phase can be accurately described by the "barometric formula". As presented in the next View 7 this is based on the expression for the model's conventional chemical

---

View 7. Barometric formula stratification. Ideal gas limit. Non-ideality correction $W(\rho,T)$, and its void-probability interpretation. Note that λ_T is the mean thermal deBroglie wavelength for the particles.

---

potential $\mu(\rho,T)$, the fundamental intensive thermodynamic property that is constant throughout the equilibrium system at number density ρ and absolute temperature *T*, in the absence of an external field. The non-ideality of that field-free system due to interparticle interactions enters $\mu(\rho,T)$ as a reversible work $W(\rho,T)$ that would be necessary to insert an additional particle anywhere within a uniform particle density ρ at temperature *T*. This quantity $W(\rho,T)$ obviously vanishes for an ideal gas (infinitely small spheres or disks). The barometric formula simply assumes that the local density $\rho(z)$ in the presence of a gravitational field corresponds to a local value of the uniform system chemical potential μ equal to the slowly varying local quantity $\mu_0 - mg(z - z_f)$, a linear function of *z* with spatial

rate of change proportional to g. Here μ_0 is a constant whose assigned value controls N, the total number of particles present in the system. Note that if the N,T,g circumstance gives rise to the presence of a crystal phase, the density profile $\rho(z)$ predicted by the barometric formula will provide no information about the crystal orientation or its long range oscillatory order, but simply specifies the crystal's average local density as a function of z. The barometric formula stratification produces an infinitely sharp fluid-crystal interface if circumstances require coexistence. In the two-dimensional hard disk case, both the fluid-hexatic and the hexatic-crystal transitions would also be represented as infinitely sharp interfaces. The former would display a density discontinuity, the latter would not but would involve a weak singularity affecting high-order z derivatives of the predicted density profile.

Strong gravitational and centrifugal fields cause rapid density changes with respect to altitude z in the system. The corresponding reversible particle insertion function W then necessarily samples a variable particle density $\rho(z)$ over a non-zero distance range σ, thus becoming a density functional $W[z,\{\rho(z')\},T]$. As can be directly verified from grand ensemble theory, this properly corrected expression for the z-dependent chemical potential is still required to conform to a linear function of altitude z. Consequently the non-local W functional is expected to be a source of non-trivial deviation from the barometric formula. The extended formalism is exhibited in the following View 8. While examining such deviations in

---

View 8. Barometric formula corrections.

---

detail, it is worth recalling the formal relation shown earlier in View 6 between the local pressure $p(z)$ (*i.e.,* from the vertical component of the stress tensor) and the now-corrected equilibrium density profile $\rho(z)$. Keep in mind that whenever there is locally a deviation from density isotropy, the stress tensor in principle should be expected to exhibit some anisotropy.

If the local density functional $W[z,\{\rho(z')\},T]$ were to be evaluated in a fluid region where $\rho(z)$ increased substantially with depth z, the lower portion of the radius-σ spherical sampling region would tend to dominate the contribution of the upper portion. This would have the effect of reducing the magnitude of the predicted density gradient compared to that predicted by the barometric formula.

Note that this local density functional correction to the barometric formula approximation has the capacity to generate vertically oscillatory

$\rho(z)$ patterns for crystal phases. But in order to do so properly it must be augmented in general with the system's relevant boundary conditions. The extension also will predict phase coexistence interfaces that are broadened from the sharp discontinuities that emerge from the barometric approximation. Crystal-phase oscillations of $\rho(z)$ determined by $W[z,\{\rho(z'\},T]$ rest primarily on the occurrence probability of finding a layer-positioned monovacancy to accommodate an inserted particle, the geometry of which strongly discriminates against insertion between layers.

By seeking a high-g equilibrium description beyond that provided by the pseudo-macroscopic barometric formula, one immediately encounters questions about crystalline order and orientation at the bottom of the system. One kind of relevant information is the crystal-fluid interfacial free energy. This has been examined for several exposed surfaces of the fcc crystal in the negligible-g situation under equilibrium coexistence conditions, with results indicated in the next View 9. Although no results are yet available

---

View 9. Crystal phase orientation: structures of the (100), (110), and (111) layers for the fcc crystal. Lowest interfacial free energy for oriented crystal in contact with fluid.

---

for large g conditions, one may tentatively assume that the relative ordering of these results persists into at least the initial portion of increasing g.

Perhaps more relevant for this crystal ordering issue is what orientation is most favorable at high g for fcc crystal contact with the assumed flat horizontal hard floor surface. In other words, which crystal orientation manages to locate particles on average closest to the floor. A straightforward numerical comparison for $T = 0$ can be produced by observing how the gravitational energy increases as crystal layers are built up sequentially from the floor, for alternative close-packed fcc crystal orientations. The gravitational energy for any chosen crystal orientation then is a piecewise linear function of the number of particles that have been added to the completing top layer. Comparing pairs of these piecewise linear results determines the favored crystal orientation. As an informative example, the next View 10 shows the occupancy dependence of the energy

---

View 10. Evidence for the preferred crystal contact orientation at the floor, $T = 0$. Displayed is the occupancy number dependence of the unit-area gravitational energy for the (100) floor-contacting orientation measured relative to that of the (111) surface orientation.

---

difference for (100) minus that for (111), displayed in reduced energy units, for a unit horizontal area. Evidently crystal surface (111) is the preferred member at least of this pair. Analogous results have been obtained for the (110) surface, again showing that the (111) energy is consistently the preferable choice as the oriented crystal is built upon the floor, but even by a substantially larger average amount. Other crystal orientations are expected to fare even worse compared to the (111) orientation. Consistent with the fluid-crystal interfacial free energy, it is clear that this analysis also supports the presumption that (111) layer orientation contacting the floor will be the lowest free energy case for $T > 0$. The two dimensional rigid disk case is simpler: The only option is that its first and subsequent layers will be the close-packed linear disk sequence.

As noted earlier, isotropic compression for the $T > 0$ fcc crystal from the coexistence pressure toward infinite pressure is accompanied by a significant reduction in the average nearest-neighbor separation. This raises the question about how disk or sphere packing geometry deals with this feature in a high-*g* situation with a substantial crystal phase at the bottom of the container. Horizontal (111) layers of spheres that nominally sit on each other, taking advantage of the underlying geometric "pockets", will be presented with numerically inconsistent lateral nearest-neighbor separations. That is, successive horizontal macroscopic layers should contain smaller numbers of particles with larger separation. The same kind of mismatching also applies to disks in two dimensions. Insertion of vacancies does not resolve this situation. However the next View 11 proposes one apparently

---

View 11. Crystal nearest-neighbor separation *vs.* altitude, and resulting packing disorder. Edge dislocations.

---

feasible option, specifically in three dimensions the inclusion of properly distributed and oriented edge dislocations in the fcc crystal phase. But note that the edge dislocations may not be oriented in a completely vertical manner. The two dimensional version of this nearest-neighbor separation requirement amounts to terminated lines of disks, each producing a dislocation at its upper end. The general conclusion is that large equilibrated hard sphere or disk crystals residing under gravitational or centrifugal fields necessarily incorporate structural defects.

An important gravitational or centrifugal phenomenon, with both commercial and international political implications, is isotope separation. For present purposes this will be discussed in the most rudimentary

modeling context, specifically a binary mixture of geometrically identical spheres or disks (common diameter σ), but distinguished by two masses $0 < m_a < m_b$. The corresponding height distributions $\rho_a(z)$ and $\rho_b(z)$ could be approximated by a binary mixture extension of the barometric distribution approximation. However the more powerful analytical approach parallels that shown earlier to correct the barometric formula approximation. Specifically it determines these individual height distributions by a coupled pair of equations that are displayed in View 12. Note that the common size

---

View 12. Isotope separation at equilibrium. Determining equations.

---

assumed for the two isotopes implies that the insertion work function W can depend only on the sum of the two local densities, not on those density distributions independently, *i.e.*, it is a functional of the form $W[z, \{\rho_a(z') + \rho_b(z')\}, T]$. The system-wide average mole fractions of the two isotopes are determined by the choices of the parameters μ_{0a} and μ_{0b} for their respective chemical potentials, both of which are linear functions of the altitude z. It should be stressed that the separation phenomenon involves more than just statistical distribution (mole fraction) of the isotopes over a density distribution determined for a single isotope case; the coupled determining equations generally produce distinct matter height distributions that are fundamentally different in shape than those exhibited by the pure-isotope cases. Obviously the heavier mass isotope is expected to concentrate toward the floor, compared to the lighter isotope concentrating toward the ceiling.

Thus far, only thermal equilibrium properties for many-hard-particle systems have been considered. There are obviously a large number of non-equilibrium properties that would command interest and attention as well. One class of irreversible phenomena that can be usefully modeled arises from dissipative sedimentation of spherical hard colloids in a viscous solvent composed of much smaller molecules, to be treated just as a surrounding continuum. A conceptually elementary version is described in the following View 13. The behavior of monodisperse colloidal suspensions driven into

---

View 13. Dissipative (over-damped) sedimentation process. Single component case. Colloid suspension applications. Multidimensional gravity gradient kinetics with frictionless constraints. Effective particle "mass" contains a solvent buoyancy contribution.

---

a sedimentary deposit in a rotating centrifuge would be an obvious connection to experiment. The presumption is that before encountering the floor or other particles in a previously formed deposit, the gravitational force on a particle causes a constant-velocity downward motion. A particle that finally comes in contact with the floor does not subsequently change its altitude z_f, but it can slide sideways if repulsive interaction with one or more descending particles makes that necessary. The full multidimensional description of dissipative (over-damped) particle motion involves self-consistent configurational relaxation in the solvent medium to lower the gravitational energy, while rigorously observing all floor and sphere (or disk) non-overlap constraints. The final result will be a static downward-jammed structure, *i.e.*, one effectively at $T = 0$.

Assuming that they all have identical effective masses, particles that are temporarily above the floor and above any sediment already deposited will move downward vertically all at the same speed. Presuming they were initially not in contact with one another, that non-contact situation therefore will persist until encounter with the floor or the deposit forming at the bottom of the system. However, when a downward-drifting particle encounters an isolated one already on the floor surface, a two-body motion that retains contact ensues. The precise details of this pair encounter are presented in View 14. The schematic figure nominally shows a pair of disks,

---

View 14. Example of a particle sliding on an isolated already-floored particle (2-dimensional view). Explicit solution in terms of reduced units.

---

but it is also applicable to hard spheres by representing a vertical plane containing the two particle centers.

The general situation requiring quantitatively precise description is that of an *n*-particle cluster connected internally by pair contacts, a particle subset of which is already in contact with the floor. Deriving quantitative details of relaxation motion for this connected cluster depend (a) on maintaining those pair and floor contacts (but allowing no others), (b) on constraining horizontal components of all particle motions so that the cluster centroid has no horizontal motion, (c) on assigning geometry-constrained force components arising from the gravitational field, and (d) on enforcing equality of the overall rate of gravitational energy reduction as the cluster relaxes, and of the net viscous friction dissipation rate. These criteria were the source of the specific motion details for the elementary $n = 2$ cluster

illustrated in View 14, and uniquely determine the kinetics of all possible $n > 2$ contact clusters.

Although every particle directly experiences the same downward gravitational force, it is important to realize that some connected sedimenting cluster geometries can temporarily require upward displacement of a particle to accommodate more intense downward motion of its neighbors. The next View 15 illustrates two examples for disks, but it

---

View 15. Upward motion examples.

---

should be clear that analogous examples also arise for hard spheres sedimenting in three dimensions.

The sedimentation process for two-dimensional hard disks will tend strongly to produce a triangular (close packed) crystal. Note that the previous concern about *z* dependence of crystal nearest-neighbor separation for $T > 0$ is not relevant for this dissipative process. Deviation from a perfect crystal structure can arise from a system width that is not exactly (or close to) an integer multiple of the diameter σ. The result will give rise to at least one grain boundary defect. But aside from that, the result is a set of simple triangular crystal domains. The corresponding three dimensional case of hard spheres is more complicated, as illustrated in the following View 16. Even if a structurally perfect first layer were to exist on the floor

---

View 16. Hard sphere crystal ambiguity (Barlow packing possibilities) and resulting disorder as sediment height increases.

---

surface due to an appropriate horizontal cross section geometry, random addition of spheres in attempting to build a second layer confronts the binary ambiguity about which subset of "pockets" provided by the bottom layer should be occupied. Such packing ambiguity underlies the infinite family of close-packed Barlow crystal structures (fcc, hcp, ...). Horizontal grain boundaries between sub-areas occupied respectively by the two pocket choices disrupt the height periodicity of subsequently sedimenting particles. The sedimentation model as defined includes no annealing mechanism to reduce that kind of packing disorder in three dimensions. At least in the three-dimensional hard sphere sedimentation case, the final static structure for random initial configurations will be amorphous, except possibly within two or perhaps three layers just above the floor. In principle one might expect the resulting amorphous gravitationally jammed packings to be statistically anisotropic, but not vividly so.

One additional feature deserves emphasis, specifically that the dissipative sedimentation process as defined will tend to avoid formation of vacancies or larger voids, at least if the initial configuration is a dilute configuration of particles. The next View 17 emphasizes schematically the nearly inevitable

---

View 17. Filling of a possible vacancy (void) by a downward sliding particle. This inhibits the formation of large rattler-containing voids. Possible exceptions to such void exclusion would require exceptionally pre-configured high density initial configurations.

---

tendency for a falling particle to drop or to slide into a vacant position, whether disks or spheres are involved. This indicates a probabilistic distinction between final configurations produced by the unidirectional sedimentation process on the one hand, and jammed amorphous hard disk or hard sphere configurations on the other hand whose conventional isotropic formation processes tend to generate a significant concentration both of monovacancies and of voids large enough to contain confined but unjammed "rattler" particles.

The description offered here for many-body gravitational effects has inevitably been very incomplete. There are many straightforward research extensions to provide more detailed qualitative and quantitative insights into the properties that have just been discussed for the classical hard sphere and hard disk models. But beyond those possibilities, the final View 18 includes

---

View 18. Additional opportunities for future research about gravitational effects.

---

a few additional scientific directions. Some of these go beyond the simple hard sphere and hard disk concepts, and include possible analytical, simulational, and even experimental, research investigations.

VIEW 1

Back

Hard Spheres under Gravity

Frank H. Stillinger

Dept. of Chemistry, Princeton University

Princeton, NJ 08544

Acknowledgements:
Galileo Galilei,
Isaac Newton,
Albert Einstein,
.....

Gravitational and Centrifugal Force Field Examples

[terrestrial gravity: $g_{terr} = 980 cm/s^2$]

Location	Field strength/g_{terr}
Orbiting space vehicle	0.0
Asteroid, 1 *km* diameter	$\approx 10^{-4}$
Earth's moon	0.166
Earth's surface	1.0
Jupiter's surface	2.53
Sun's surface	28.0
Ultracentrifuge	$\approx 10^{6}$
Neutron star surface	$\approx 10^{11}$

^{132}Xe Elevation Change
Requiring Energy $k_B T|_{298K} = 4.1143 \times 10^{-14}$ *erg*

Location	Altitude increase, *cm*
Orbiting space vehicle	$+\infty$
Asteroid, diameter 1 *km*	$\approx 1.92 \times 10^{9}$
Earth's moon	1.15×10^{6}
Earth's surface	1.92×10^{5}
Jupiter's surface	7.58×10^{4}
Sun's surface	6.85×10^{3}
Ultracentrifuge	≈ 0.192
Neutron star surface	$\approx 1.92 \times 10^{-6}$

Hard Sphere Equilibrium Equation of State, Zero Gravity

- Hard sphere diameter σ . Pressure equation of state (classical):

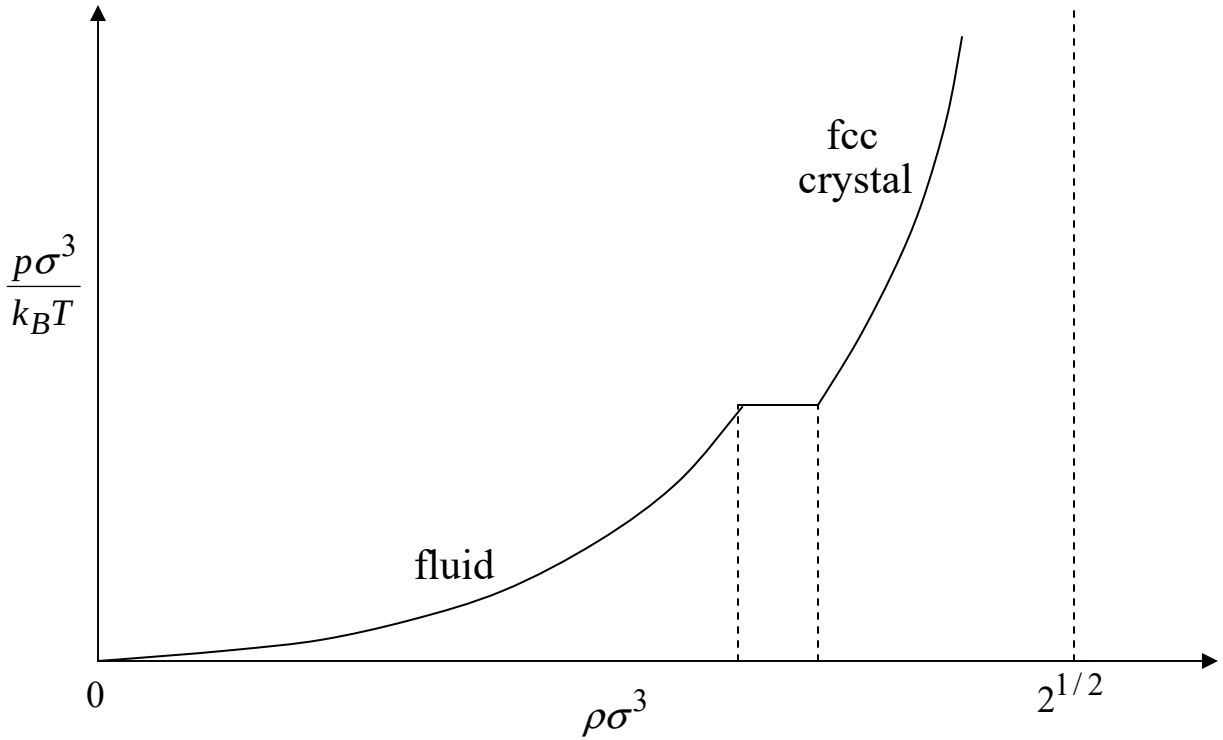

- Phase transition parameters: $(p\sigma^3/k_BT)_{coex} \cong 11.57$,

$(\rho\sigma^3)_{fluid} \cong 0.938$, $(\rho\sigma^3)_{fcc} \cong 1.037$.

- Average nearest neighbor separation in fcc crystal at its melting point: 1.109σ .

Hard Disk Equilibrium Equation of State, Zero Gravity

- Hard disk diameter σ. Pressure equation of state (classical):

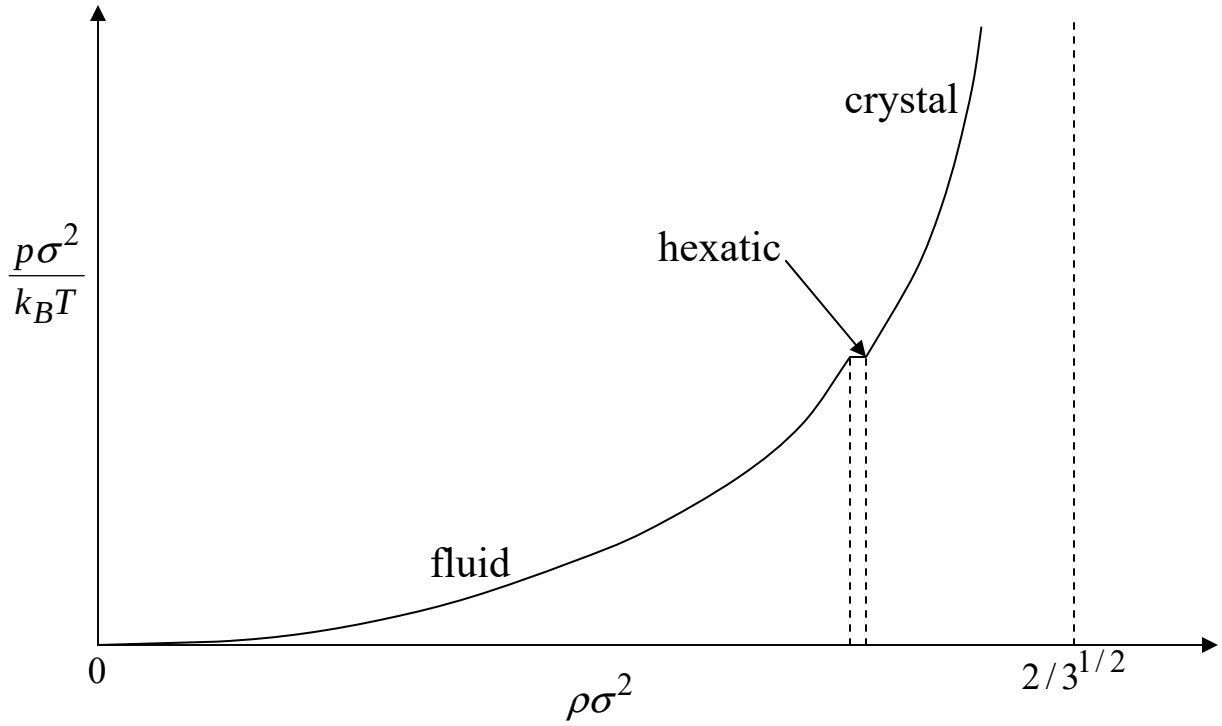

- First-order fluid-hexatic transition parameters: $(p\sigma^2/k_BT)_{fluid-hex} \cong 9.185$,
$(\rho\sigma^2)_{fluid} \cong 0.891$, $(\rho\sigma^2)_{hex} \cong 0.913$.
- Higher-order hexatic-crystal transition parameters:
$(p\sigma^2/k_BT)_{hex-cryst} \cong 9.469$, $(\rho\sigma^2)_{hex-cryst} \cong 0.917$.
- Average crystal nearest-neighbor separation at crystal-hexatic melting: 1.122σ .

Field-Oriented Macroscopic Container Geometry

- Rectangular container, z direction parallel to field direction, impenetrable floor (z_f) and ceiling (z_c), lateral direction periodic boundary conditions, fixed horizontal cross section area A:

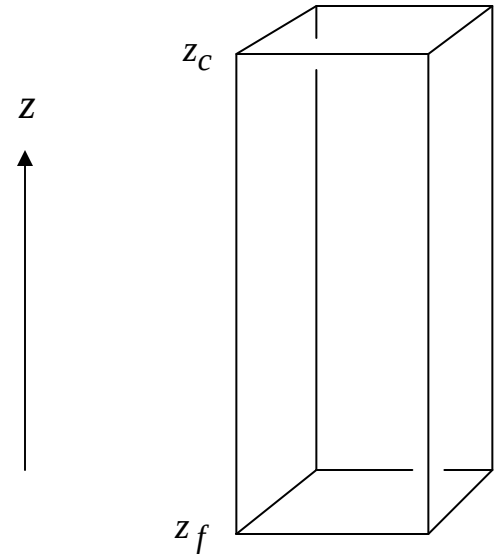

- Gravitational potential energy: $\Phi_g(\mathbf{r}_1,...,\mathbf{r}_N) = mg \sum_{j=1}^{N} (z_j - z_f)$.

- Vertical pressure via density distribution $\rho(z)$: $p(z) = p(z_c) + mg\int_z^{z_c} \rho(z')dz'$.

Barometric Formula Stratification

- Exact $\mu(\rho, T)$ includes reversible isothermal particle insertion work *W*:

$$\mu(\rho,T) = k_B T \ln(\rho\lambda_T{}^3) + W(\rho,T)$$

which formally includes all non-ideal fluid and phase change detail.

- For hard spheres (disks), $\exp[-W(\rho,T)/k_B T]$ equals the probability that a radius-σ sphere (circle) is devoid of particle centers.

- For weak gravity, assume local thermodynamic equilibrium, with a *z*-dependent chemical potential:

$$\mu[\rho(z),T] = \mu_0 - mg(z - z_f)$$

- μ_0 is a *z*-independent constant that controls the system's occupancy number *N*.

- Ideal gas approximation $\mu(\rho,T) \approx k_B T \ln(\rho\lambda_T{}^3)$ yields exponential distribution:

$$\rho(z) \propto \exp[\, -mg\,(z - z_f)/k_B T\,]$$

- Implications of general barometric formula with exact $\mu(\rho, T)$:
  - (A) Crystal phases represented only by monotonic $\rho(z)$;
  - (B) Interfaces between coexisting phases are infinitely sharp.

Barometric Formula Deficiencies / Corrections

- Height variation of $\rho(z)$ for large g requires a non-local insertion work functional W in the chemical potential:

$$\mu(z,T) = k_B T \ln[\rho(z)\lambda_T{}^3] + W[z,\{\rho(z')\},T]$$

which must involve a density stratification causing it to equal $\mu_0 - mg(z - z_f)$.

- For spheres (disks) $\exp[-W[z,\{\rho(z')\},T]/k_B T]$ equals the probability that a sphere (circle) of radius σ centered at height z is devoid of particle centers.

- This radius-σ local sampling in the fluid phase is biased toward the higher density (lower altitude) portion of the exclusion region, producing less rapid height variation of $\rho(z)$.

- The non-local character of $W[z,\{\rho(z')\},T]$ can generate oscillatory density profiles needed for description of oriented crystal phases.

Crystal-Phase Layer Orientations and Patterns

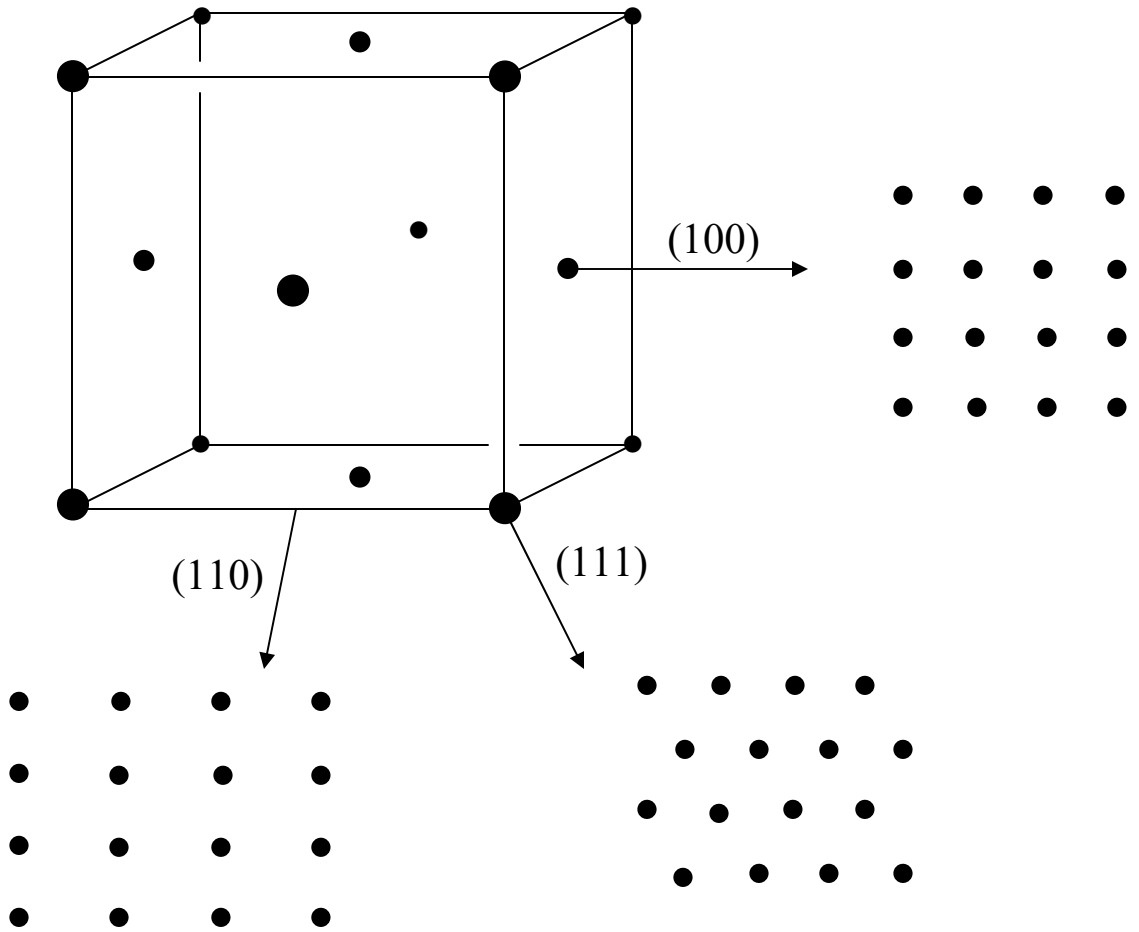

- For hard sphere fluid-crystal coexistence at $g = 0$, the most stable planar interface involves the (111) surface [R.L. Davidchack, J. Chem. Phys. **133**, 234701 (2010).]

Crystal Phase Orientation Preference

- Gravitational energy *vs.* crystal-layer sequential-depositing population is a piecewise-linear function. This plot shows the deposition energy difference for (100) minus (111) in reduced units:

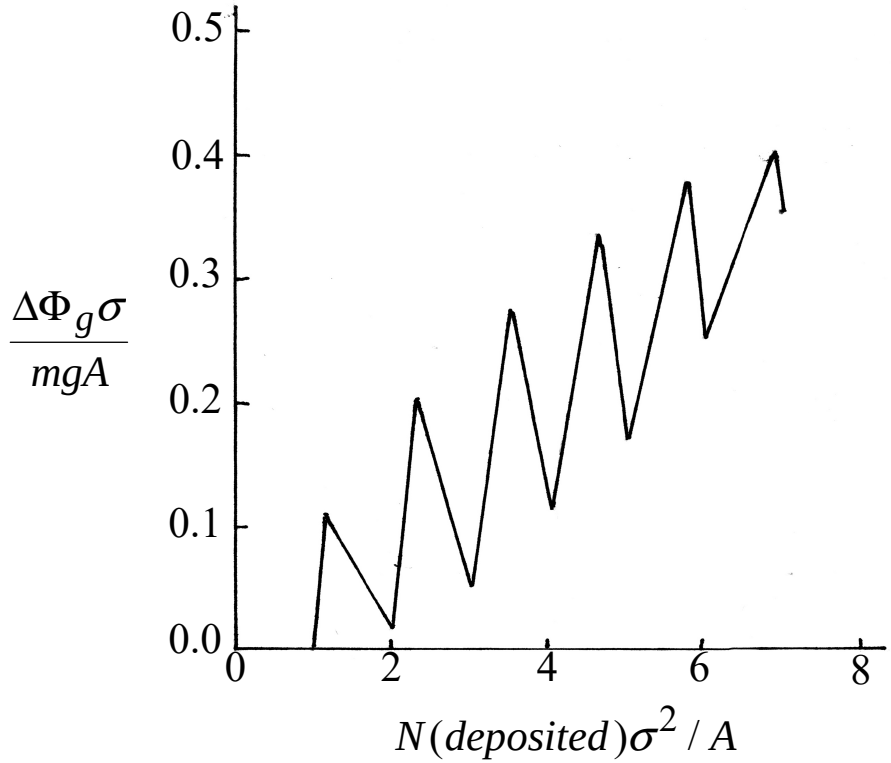

- Corresponding plot of gravitational energy difference for (110) and (111) orientations shows an even greater relative stability of the latter.
- Other orientations are expected to do even worse compared to (111), suggesting it is the preferred crystal orientation at high g, $T > 0$.

Crystal Nearest-Neighbor Separation *vs.* Altitude

- In a high-g, $T > 0$ system containing a deep section of crystal phase, the nearest-neighbor separation can decrease near its top from $\approx 1.1\sigma$ near its top to $\approx \sigma$ near its bottom.
- Successive horizontal layers with slightly different spacings do not fit together properly.
- Properly oriented edge defects can produce a coarse resolution of the mismatch:

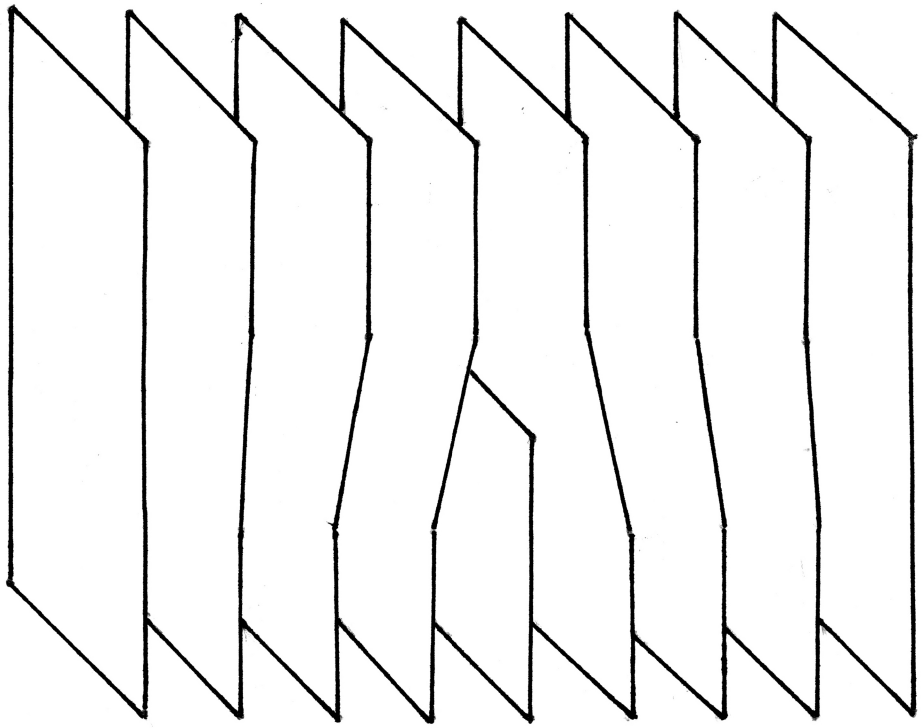

Isotope Separation

- "Isotopes" a and b: Spheres (or disks) with common diameter σ, but unequal masses $m_a < m_b$.

- Separate vertical density profiles $\rho_a(z)$ and $\rho_b(z)$:

$$N_a = A\int_{z_f}^{z_c} \rho_a(z')dz' \quad , \qquad N_b = A\int_{z_f}^{z_c} \rho_b(z')dz' \quad ,$$

where A is the constant horizontal cross-section area (length) of the container.

- Coupled determining equations:

$$k_B T \ln[\rho_a(z)\lambda_{Ta}{}^3] = \mu_{0a} - m_a g(z - z_f) - W[z, \{\rho_a(z') + \rho_b(z')\}, T] \quad ,$$

$$k_B T \ln[\rho_b(z)\lambda_{Tb}{}^3] = \mu_{0b} - m_b g(z - z_f) - W[z, \{\rho_a(z') + \rho_b(z')\}, T] \quad .$$

- The constants μ_{0a} and μ_{0b} control N_a and N_b .

- Insertion free energy functional W depends only on $\rho_a(z') + \rho_b(z')$, not the individual density profiles.

Dissipative Sedimentation Process

- Spherical (or circular) colloids initially suspended in container with viscous solvent:

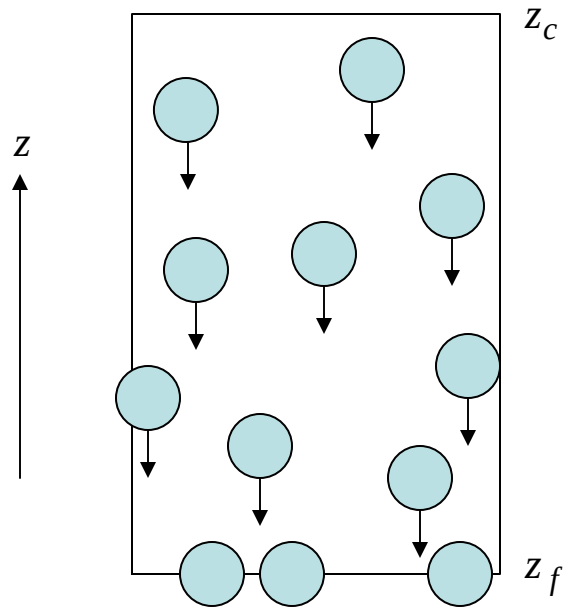

- Unimpeded downward drift speed is mg/ζ, $m =$ eff. mass, $\zeta =$ friction coeff.
- A particle at z_f cannot subsequently move upward, but it can slide sideways.
- Particle collision trajectories with already deposited sediment particles are dynamically determined by interparticle forces and floor constraints.

Particle Sliding During Sediment Contact

- Natural units to describe sedimentation kinetics:
  length $l_0 = \sigma$, energy $\varepsilon_0 = mg\sigma$, time $t_0 = \zeta\sigma / mg$.

- Particle (2) encountering already-floored particle (1):

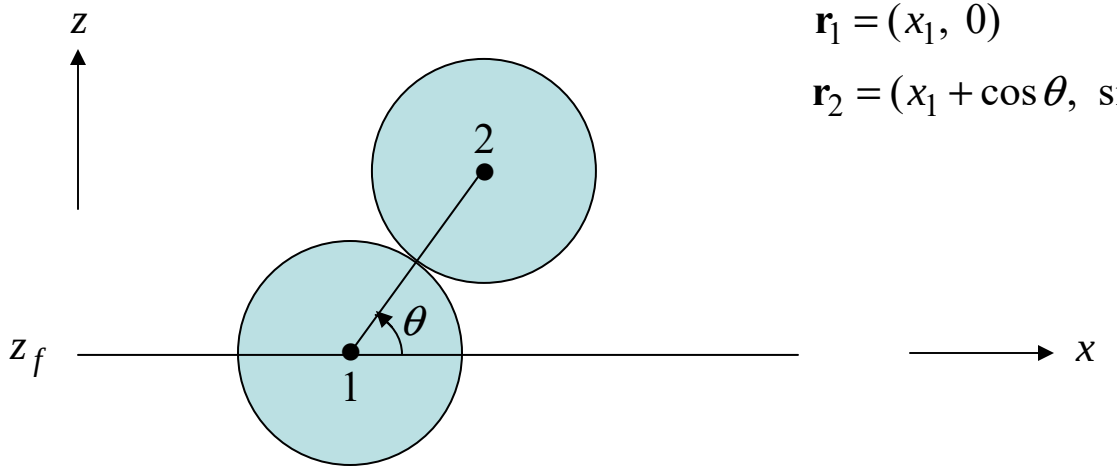

$\mathbf{r}_1 = (x_1,\ 0)$

$\mathbf{r}_2 = (x_1 + \cos\theta,\ \sin\theta)$

- Explicit (reduced unit) time dependence of particle positions:

$$\frac{dx_1}{dt} = -\frac{dx_2}{dt} = -\frac{\tan\theta}{2 + \tan^2\theta} \quad , \qquad \frac{dz_2}{dt} = -\frac{2}{2 + \tan^2\theta} \quad .$$

Cooperatively Enforced Upward Displacement

- Isolated trimer, roughly vertical orientation above a floor contact:

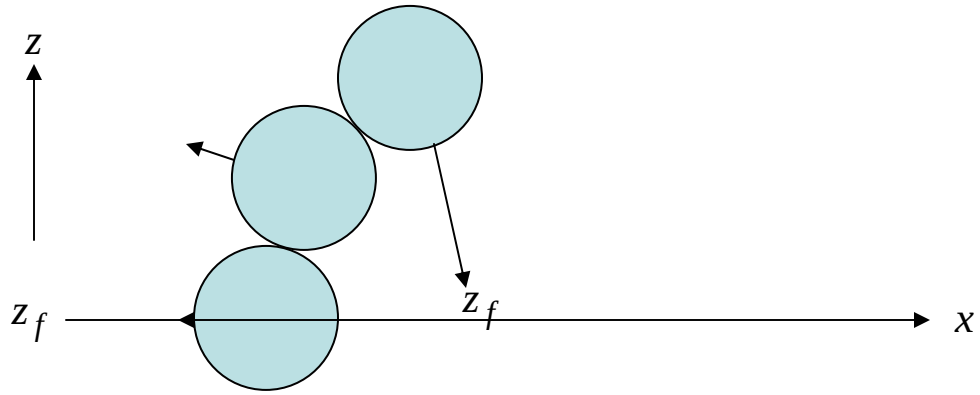

- Unequal competition for floor space between large, nearly immovable floor clusters:

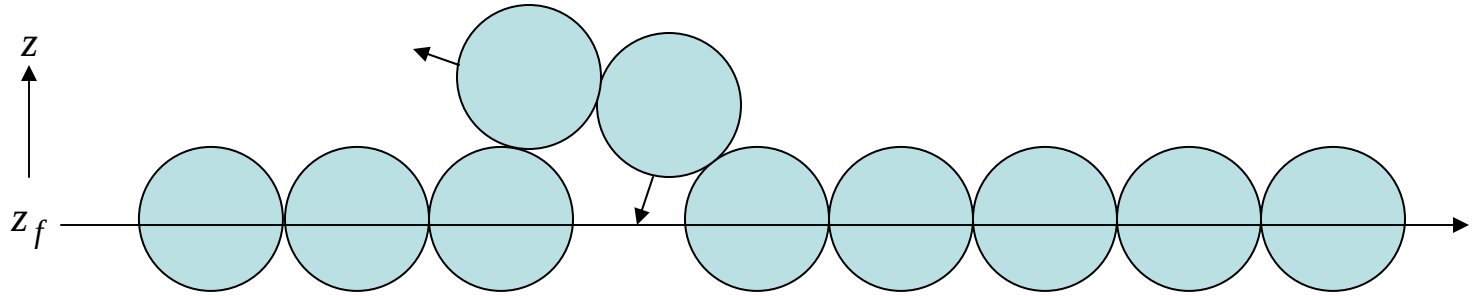

Hard Sphere Crystal Packing Ambiguity (Local Barlow Degeneracy)

- Close packed (111) layer at z_f presents a binary choice of equivalent pockets (B *vs.* C) either of which can be occupied by subsequently depositing particles:

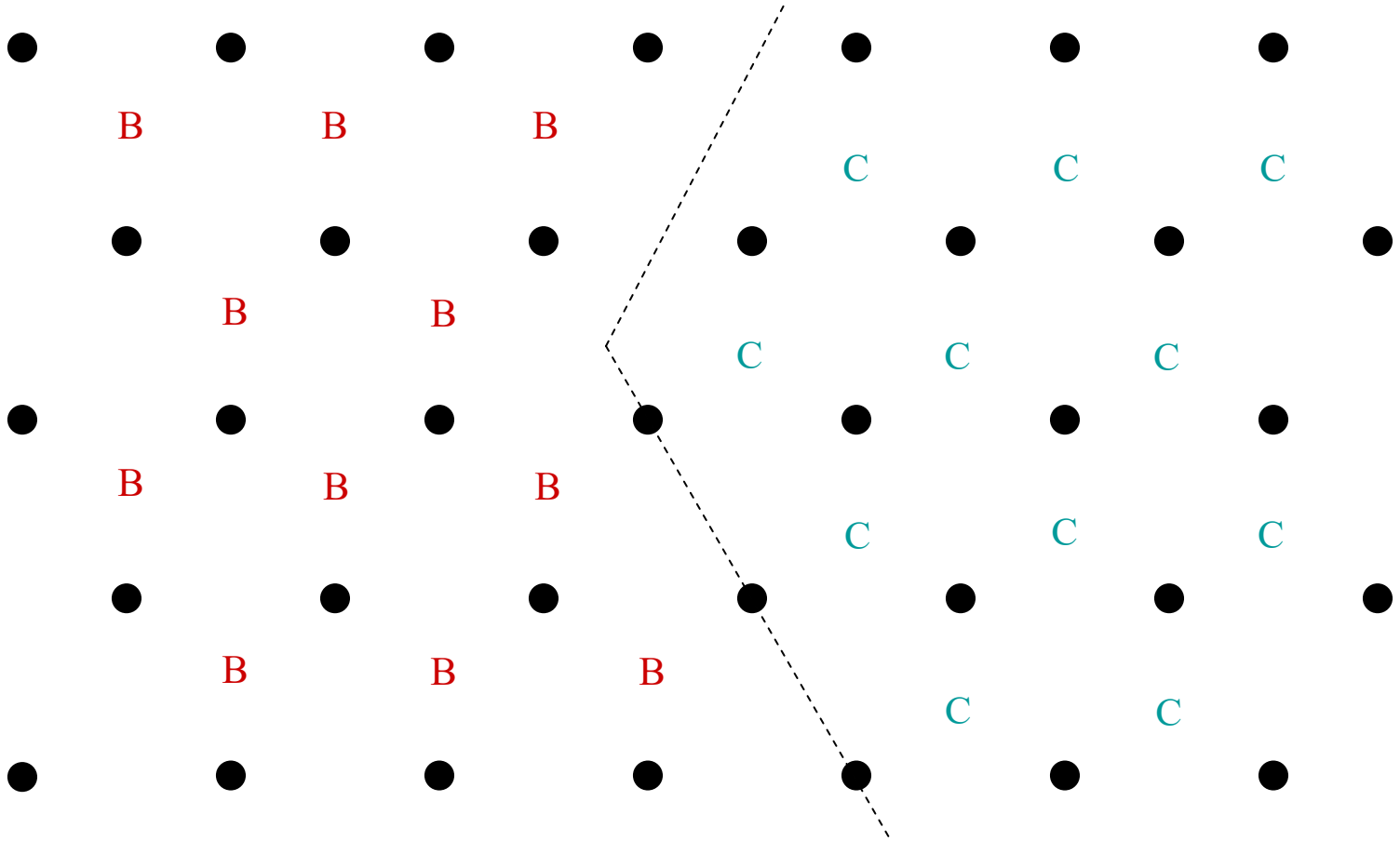

- Partially open boundaries between B and C zones disrupt subsequent layer heights.

Vacancy and Rattler Discrimination

- Unidirectional sedimentation at low colloid density fills partially formed voids. This occurs before a “roof” of particles can form over that empty location.

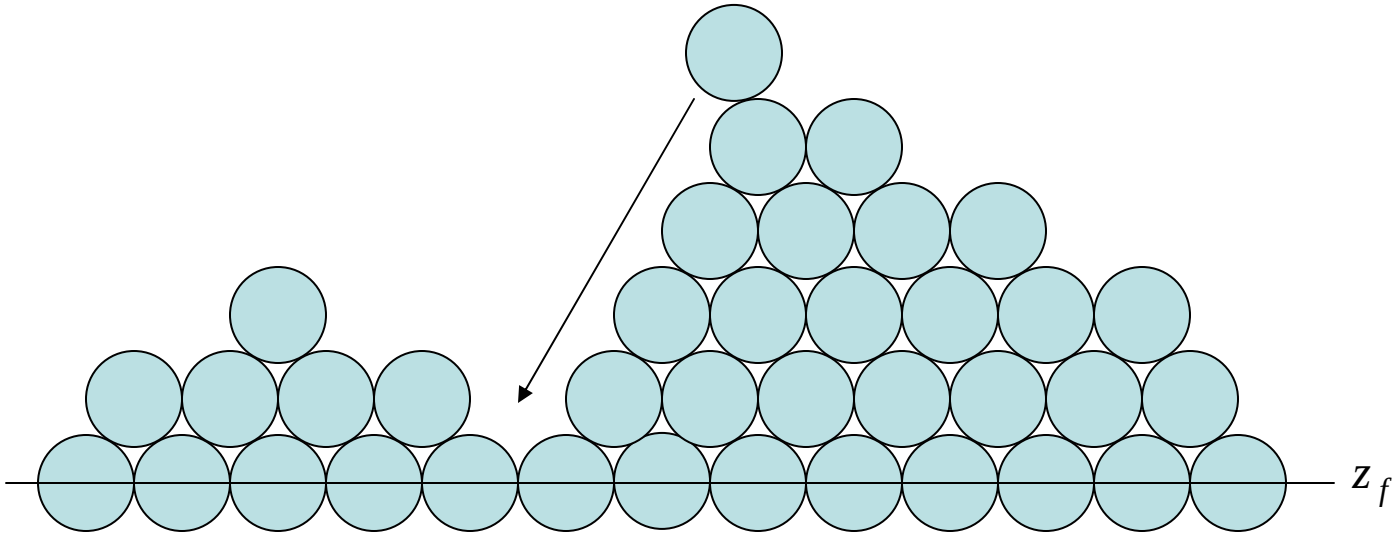

- In contrast to conventional isotropic jamming algorithms, this strongly suppresses appearance of imprisoned “rattler” particles.

Research Opportunities, Gravitational Effects

- Hard sphere and disk diffusion kinetics (inverted parabolic orbits).
- Sedimentation model extensions that involve polydisperse hard-particle colloids, with distinct radii and effective masses.
- Block copolymer configurational preferences, with distinct monomer masses.
- Gravitational stratification of systems exhibiting negative volume of melting, and those with inverse melting.
- Gravitational phenomena for hard sphere bosons as $T \to 0$, including superfluidity.
- Electric fields induced by strong gravity acting on ionic systems with substantially different anion and cation masses.